BIOCHEMISTRY
including biophysical chemistry & molecular biology

Article

pubs.acs.org/biochemistry

Cofactor-Dependent Structural and Binding Properties of Yeast Cytochrome *c* Peroxidase

Yann G. J. Sterckx[†,‡] and Alexander N. Volkov*[,‡,§]

[†]Research Unit for Cellular and Molecular Immunology (CMIM), Vrije Universiteit Brussel, Pleinlaan 2, 1050 Brussels, Belgium
[‡]Structural Biology Research Center, VIB, Pleinlaan 2, 1050 Brussels, Belgium
[§]Jean Jeener NMR Centre, Structural Biology Brussels, Vrije Universiteit Brussel, Pleinlaan 2, 1050 Brussels, Belgium

ABSTRACT: Yeast cytochrome *c* peroxidase (CcP) is a heme enzyme that reduces hydroperoxides using the electrons provided by its physiological partner cytochrome *c* (Cc). Contributing to the resistance against the oxidative stress associated with the aerobic metabolism, the Cc−CcP complex has been widely studied and became a paradigm for biological electron transfer. The heme-free, enzymatically inactive apo CcP is the natural precursor of the mature, cofactor-bound holo protein. Despite its physiological relevance, apo CcP is not well characterized, and at present, little is known about its structure or the interaction with Cc. Using a range of biophysical techniques, here we show that, while holo CcP binds Cc with micromolar affinity, the interaction between apo CcP and Cc is completely abolished. Characterized by small-angle X-ray scattering, solution nuclear magnetic resonance spectroscopy, and equilibrium unfolding experiments, apo and holo CcP exhibit very similar structural, hydrodynamic, and thermodynamic properties. However, detailed analysis reveals that apo CcP is more expanded in solution, displays a number of characteristics associated with a molten globule state, and, unlike the holo protein, does not form an unfolding intermediate during thermal and chemical denaturation. Overall, our data suggest that the Cc binding site present in the holo protein is disrupted in the apo form, explaining the inability of the latter to interact with Cc. We argue that the observed difference in Cc binding is physiologically relevant and suggest why abolishing the apo CcP−Cc interaction is beneficial to the organism.

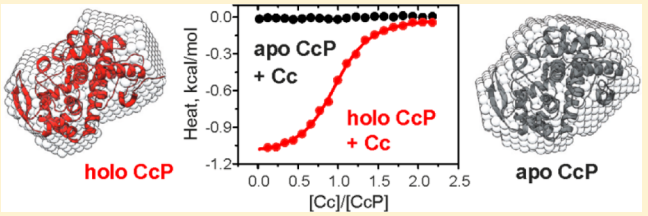

Located in the mitochondrial intermembrane space, yeast cytochrome *c* peroxidase (CcP) is a 34.2 kDa heme enzyme that catalyzes reduction of hydroperoxides using the electrons provided by its physiological partner cytochrome *c* (Cc).[1] The catalytic mechanism of H_2O_2 reduction involves formation of CcP compound I (CpdI), an intermediate oxidized 2 equiv above the CcP(Fe^{3+}) resting state and containing the Fe(IV)═O heme oxyferryl and W191 cation radical. Subsequent CpdI reduction in two one-electron steps involves complex formation with ferrous Cc, intermolecular electron transfer (ET), and product dissociation.[1] Although CcP is not essential for the viability and respiration of *Saccharomyces cerevisiae*, it contributes to the resistance against the oxidative stress associated with aerobic metabolism, mainly through its enzymatic activity as part of the Cc−CcP system (ref 2 and references cited therein).

Discovered more than 70 years ago,[3] CcP has been widely investigated and is the first heme enzyme whose structure was determined by X-ray crystallography.[4] The protein contains a *b*-type, noncovalently bound heme group, ligated by a histidine residue and featuring a vacant coordination position available to the substrate or small ligands. Removal of the cofactor from the native, holo protein yields the heme-free, enzymatically inactive apo CcP.[5] Produced in yeast under anaerobic growth conditions, apo CcP is converted to the holo form upon exposure to oxygen during aerobic respiration, thus acting as the natural precursor of the mature enzyme.[6,7] Although being clearly physiologically relevant, apo CcP has been studied much less than the holo protein, and its structure is not known.

Since the first demonstration in 1971 by Nicholls and Mochan that holo CcP binds Cc *in vitro*,[8] this protein complex has been extensively studied and become a paradigm for understanding biological ET.[1,2] The holo CcP−Cc interaction has been characterized by a variety of biophysical techniques (reviewed in ref 2), and the structure of the complex was determined by X-ray crystallography[9] and later confirmed by solution nuclear magnetic resonance (NMR) spectroscopy.[10] In contrast, to the best of our knowledge, no report assessing the binding of Cc to apo CcP has ever been published. Given that these two proteins are produced in yeast under normal physiological conditions and colocalize in the same cellular compartment, their interaction *in vivo* appears to be possible as it satisfies both spatial and temporal constraints. Thus, characterizing apo CcP−Cc binding could shed light on the mechanism of regulation of the Cc−CcP antioxidant activity.

Here, we present a comparative study of apo and holo CcP and their interactions with Cc in solution by a combination of biochemical and biophysical techniques. First, using isothermal titration calorimetry (ITC), surface plasmon resonance (SPR),

Received: May 19, 2014
Revised: June 25, 2014
Published: June 25, 2014

   dx.doi.org/10.1021/bi500603w | *Biochemistry* 2014, 53, 4526−4536

and NMR spectroscopy, we show that while holo CcP binds Cc with a micromolar affinity, the interaction between apo CcP and Cc is completely abolished. To understand the reason for such a dramatic difference in their binding properties, we characterized both CcP forms by small-angle X-ray scattering (SAXS), heteronuclear NMR spectroscopy, and equilibrium unfolding experiments. At first glance, apo and holo CcP exhibit very similar structural, hydrodynamic, and thermodynamic properties; however, detailed analysis reveals that apo CcP is more expanded in solution, displays a number of characteristics associated with a molten globule state, and, unlike the holo protein, does not form an unfolding intermediate during thermal and chemical denaturation. Overall, our data suggest that the Cc binding site present in the holo protein is disrupted in the apo form, explaining the inability of the latter to interact with Cc. Finally, we argue that the difference in Cc binding seen for holo and apo CcP is physiologically relevant and suggest why abolishing the apo CcP−Cc interaction is beneficial to the organism.

MATERIALS AND METHODS

Protein Samples. Both natural-abundance and uniformly labeled [^{2}H,^{15}N]CcP and [^{15}N]Cc were prepared as described previously.[11,12] Purified Cc was oxidized with an excess of $K_3[Fe(CN)_6]$ and thoroughly exchanged into the working buffer. The protein concentrations were calculated from the UV−vis spectra using the following extinction coefficients: ε_{280} = 59.4 mM^{-1} cm^{-1} (apo CcP),[12] ε_{408} = 98.0 mM^{-1} cm^{-1} (holo CcP),[13] and ε_{410} = 106.1 mM^{-1} cm^{-1} (oxidized Cc).[14]

NMR Spectroscopy. NMR samples with protein concentrations of 0.22−0.7 mM were prepared in 20 mM sodium phosphate (NaP_i) and 100 mM NaCl (pH 6.0 or 7.0) and contained 6% ^2H_2O for the lock. The two-dimensional ^{1}H−^{15}N HSQC experiments (TROSY-selected in the case of the [^{2}H,^{15}N]CcP samples) were conducted on Varian NMR Direct-Drive System 600 and 800 MHz spectrometers, the latter equipped with a salt-tolerant triple-resonance PFG-Z cold probe. All NMR data were processed in NMRPipe[15] and analyzed in CCPN.[16] Chemical shift assignments of the Cc resonances were taken from the literature.[11] The average amide chemical shift perturbations ($\Delta\delta$) were calculated with the equation $\Delta\delta = (\Delta\delta_N^2/50 + \Delta\delta_H^2/2)^{0.5}$, where $\Delta\delta_N$ and $\Delta\delta_H$ are the chemical shift perturbations of the amide nitrogen and proton, respectively.

Electronic Absorption and Circular Dichroism Spectroscopy. The electronic absorption spectra were recorded on a Cary 100 Bio (Varian) spectrophotometer at 25.0 ± 0.2 °C in 20 mM NaP_i, 100 mM NaCl (pH 6.0), and protein concentrations of 0.8−2.0 μM. Continuous scans in the region of 250−750 nm were taken using a 1 cm cuvette, a scan rate of 600 nm/min, a bandwidth of 2.0 nm, and a resolution of 1 nm. The extinction coefficient of the Soret band of the resting state CcP used to calculate the protein concentration was taken from previous work.[12]

Far-UV CD spectra were recorded on a J-715 spectropolarimeter (Jasco) in 20 mM NaP_i, 100 mM NaCl (pH 6.0), and a CcP concentration of 2 μM. For the native and urea-denatured proteins, continuous scans in the region of 200−240 nm were taken using a 1 mm cuvette, a scan rate of 50 nm/min, a bandwidth of 1.0 nm, and a resolution of 0.5 nm, with the CD spectra averaged over six consecutive scans. The raw CD data (ellipticity θ in millidegrees) were normalized for protein concentration and the number of residues, yielding the mean residue ellipticity ($[\theta]$ in degrees square centimeters per mole): $[\theta] = (\theta M_r)/(nCl)$, where M_r, n, C, and l are the molecular mass (daltons), the number of CcP residues, the protein concentration (in milligrams per milliliter), and the cuvette path length (in centimeters), respectively.

Thermal unfolding experiments were performed by increasing the temperature from 19.10 to 86.00 °C at a constant rate of 0.84 °C/min. To monitor the changes in the α-helical content, the ellipticity at 222 nm was registered every 0.14 °C, corresponding to a sampling rate of 6 min^{-1}. The unfolding curves were normalized prior to analysis.

Fluorescence Spectroscopy. The fluorescence experiments were conducted on a PerkinElmer LS55 luminescence spectrometer at 25.0 ± 0.1 °C in 20 mM NaP_i and 100 mM NaCl (pH 6.0) with a cuvette path length of 1 cm. Following excitation at 295 nm, the tryptophan fluorescence emission spectra were acquired in the range of 300−400 nm, with excitation and emission slit widths of 3 or 4 nm and protein concentrations of 0.56−0.90 μM. The fluorescence emission of 8-anilinonaphthalene-1-sulfonic acid (ANS) in the range of 400−650 nm was recorded following excitation at 350 nm, with excitation and emission slit widths of 5 and 4 nm, respectively, and protein and ANS concentrations of 1.0 and 50.0 μM, respectively. All spectra were acquired with a scan rate of 100 nm/min and a resolution of 0.5 nm and were averaged over three consecutive scans. At each denaturant concentration, the fluorescence spectrum in the absence of the protein was recorded and subtracted from the corresponding spectrum of the protein sample, with the resulting difference curve providing the position of the emission maximum (λ_{max}) and the corresponding fluorescence intensity (F_{max}) used in the subsequent analysis. Upon addition of the denaturant, all samples were allowed to equilibrate for several hours at room temperature prior to the fluorescence measurements.

To obtain the equilibrium dissociation constant (K_D) for the binding of ANS to apo CcP, a series of fluorescence emission spectra at a constant ANS concentration (10 μM) and varying CcP concentrations (1−100 μM) were recorded, and the data were analyzed with the binding model adapted from ref 17 (eq 1):

$$[\mathrm{CcP}] = \frac{F}{F_0}([\mathrm{ANS}] + K_D) + K_D\left[\left(\frac{F}{F_0}\right)^2 + \left(\frac{F}{F_0}\right)^3\right] \quad (1)$$

where [CcP] and F are the protein concentration and the ANS fluorescence signal at a given titration point, respectively, [ANS] is the total ANS concentration (held constant throughout the titration), F_0 is the fluorescence signal of the ANS fully bound to the protein, and K_D is the equilibrium dissociation constant. Equation 1 assumes the 1:1 binding stoichiometry, which is the case for the apo CcP−ANS interaction.[18]

Equilibrium Protein Unfolding. Thermal and chemical denaturation curves were analyzed with two-state unfolding models (eqs 2 and 3, respectively):[19]

$$y_{obs} = \frac{y_N + a_N T}{1 + \exp\left(\frac{\Delta H_m}{RT_m} - \frac{\Delta H_m}{RT}\right)} + \frac{(y_U + a_U T)\exp\left(\frac{\Delta H_m}{RT_m} - \frac{\Delta H_m}{RT}\right)}{1 + \exp\left(\frac{\Delta H_m}{RT_m} - \frac{\Delta H_m}{RT}\right)} \quad (2)$$

dx.doi.org/10.1021/bi500603w | Biochemistry 2014, 53, 4526−4536

where y_{obs} is the signal observed at temperature T, R is the absolute gas constant, $y_N + a_N T$ and $y_U + a_U T$ are the linear slopes of the pre- and post-transitional regions of the unfolding curve, respectively, and ΔH_m is the change in enthalpy at the transition temperature, T_m:

$$y_{obs} = \frac{y_N + a_N C}{1 + \exp\left(\frac{mC - \Delta G_{H_2O}}{RT}\right)} + \frac{(y_U + a_U C)\exp\left(\frac{mC - \Delta G_{H_2O}}{RT}\right)}{1 + \exp\left(\frac{mC - \Delta G_{H_2O}}{RT}\right)} \quad (3)$$

where y_{obs} is the signal observed at the concentration of the denaturant C, ΔG_{H_2O} is the free energy change in the absence of denaturant, m is the value that reflects the steepness of the unfolding transition, and $y_N + a_N C$ and $y_U + a_U C$ are the linear slopes of the pre- and post-transitional regions of the unfolding curve, respectively. The denaturant concentration at the transition midpoint, C_m, is given by the equation $C_m = \Delta G_{H_2O}/m$.

Isothermal Titration Calorimetry. Experiments were performed at 25.00 ± 0.01 °C on an ITC200 calorimeter (GE Healthcare). The protein samples were extensively dialyzed against 20 mM NaP_i and 100 mM NaCl (pH 6.0) and degassed before being used. Ferric Cc (1 mM) was titrated into a 100 μM solution of either apo or holo CcP. Titrations were performed with a preliminary injection of 0.8 μL, followed by 20 injections of 2 μL, a delay between injections of 210 s, an initial equilibration delay of 120 s, and a syringe rotation speed of 800 rpm. In each case, the first data point was discarded and the baseline adjusted manually, and the integrated data were fit to a binding model assuming n identical and independent sites.[20]

Surface Plasmon Resonance. The experiments were conducted on a BIAcore 2000 platform (GE Healthcare) at 25.0 ± 0.1 °C with 20 mM NaP_i, 100 mM NaCl (pH 6.0), and 0.005% Tween 20 as the running buffer. Holo or apo CcP was immobilized on a CM5 sensor chip (GE Healthcare) in flow cell 2 using the following amine coupling procedure. First, the carboxylated dextran matrix was activated by a solution of 0.2 M *N*-ethyl-*N*′-[3-(diethylamino)propyl]carbodiimide (EDC) and 0.05 M *N*-hydroxysuccinimide (NHS) injected for 7 min at a flow rate of 5 μL/min. Then, a CcP solution [40 μg/mL in 20 mM NaP_i and 100 mM NaCl (pH 4.7)] was injected until the desired amount of protein was immobilized (~280 response units). Finally, the remaining activated surface was blocked by a 7 min injection of 1 M ethanolamine hydrochloride. Used as a reference, the surface in flow cell 1 was treated with only EDC, NHS, and ethanolamine. The desired amount of the coupled ligand (R_L) was calculated using the equation $R_L = (R_{max}M_L)/(nM_A)$, where R_{max} is the maximal binding response, n is the binding stoichiometry, and M_A and M_L are the molecular weights of the analyte (Cc, 12 kDa) and ligand (CcP, 34 kDa), respectively.

The sensorgrams at different Cc concentrations (0.5, 0.75, 1, 2.5, 5, 10, 20, 30, and 40 μM for holo CcP and 2.5, 5, 10, 30, 50, 100, 250, and 500 μM for apo CcP), as well as the zero-concentration reference (injection of the running buffer), were recorded at a flow rate of 30 μL/min and a sampling rate of 2 Hz. Analyte injections were performed with 60 μL KINJECTs. In the case of holo CcP, the dissociation proceeded for 600 s, which also served as the regeneration condition. For apo CcP, the dissociation phase lasted for 120 s, which was followed by a 15 μL pulse injection of the regeneration buffer [50 mM Tris-HCl and 500 mM NaCl (pH 8.0)]. While the data for apo CcP were collected in triplicate, multiple Cc injections could not be performed for holo CcP because of the limited lifetime of the latter on the CM5 chip.

For the equilibrium analysis, the reference and zero-concentration data were subtracted from the sensorgrams, the response values at equilibrium (R_{eq}) were determined for each analyte concentration, and the data were analyzed with the equilibrium binding model $R_{eq} = (R_{max}[Cc])/(K_D + [Cc])$, where [Cc] is the analyte concentration and K_D the equilibrium dissociation constant.

Small-Angle X-ray Scattering. All experiments were conducted on beamline ID14-3 (ERSF, Grenoble, France). Prior to analysis, the samples were exhaustively dialyzed against 20 mM NaP_i, 100 mM NaCl, and 5 mM ascorbate (pH 6.0). Some of the dialysis buffer was passed through a 0.22 μm filter and kept as a reference for the subsequent experiments. For both holo and apo CcP, aliquots of the samples were prepared at different concentrations (2, 4, 7, and 10 mg/mL) by diluting the concentrated protein stock with the filtered dialysis buffer. Scattering curves were collected at the different protein concentrations, and the blank buffer measurements were performed before and after each experiment. The samples were kept at 15.0 ± 0.1 °C prior to data collection and exposed for 5 s to the beam with a transmission level of 50%.

The collected SAXS data were processed and analyzed with the ATSAS package.[21] Comparison of the scattering curves obtained after buffer subtraction revealed a slight concentration dependency for both apo and holo CcP. The scattering curves were analyzed and merged accordingly to obtain final zero-concentration scattering curves through extrapolation.[22,23] These extrapolated curves were thoroughly examined using the ATSAS package,[21] Scatter,[24] and the online SAXSMoW application.[25] The final scattering curves were also used for the *ab initio* modeling. Briefly, 18 *ab initio* models were generated by DAMMIF[26] and averaged using DAMAVER.[27] A starting bead model was extracted from the averaged dummy-atom model for the calculation of a final model in DAMMIN.[28] The theoretical scattering curves of apo and holo CcP were generated from the high-resolution X-ray structure [Protein Data Bank (PDB) entry 2ZBY][29] and compared to the experimental SAXS data sets using CRYSOL.[30] The information on data collection and derived structural parameters is given in Table 1 according to the guidelines provided by Jacques et al.[31]

RESULTS

Cc Binding. Amenable to a wide variety of biophysical techniques, the interaction of Cc with holo CcP has been extensively studied.[2] In agreement with the values reported in the literature, the K_Ds determined here for the binding of Cc to holo CcP by ITC and SPR are 4.8 ± 0.2 and 6.4 ± 0.2 μM, respectively. At the same time, no binding of Cc to apo CcP was observed by either of these techniques (Figure 1A,B). This finding is further confirmed by NMR chemical shift perturbation analysis, employing isotopically labeled [^{15}N]Cc and natural abundance CcP. The interaction of [^{15}N]Cc with holo CcP leads to changes in the spectral positions of the Cc resonances affected by the binding, resulting in a distinct pattern in chemical shift perturbation plots (Figure 1C, left). In contrast, addition of apo CcP has no effect on the NMR spectrum of [^{15}N]Cc, yielding an

dx.doi.org/10.1021/bi500603w | *Biochemistry* 2014, 53, 4526−4536

Table 1. SAXS Data Collection and Scattering-Derived Parameters

Data Collection Parameters		
beamline	ID14-3[55]	
wavelength (Å)	0.93	
q range (Å^{-1})	0.004−0.612	
exposure time (s)	5	
beam transmission (%)	50	
no. of frames collected	10	
concentration (mg/mL)	2, 4, 7, 10	
temperature (°C)	15	
secondary standards used	BSA	
Structural Parameters		
	holo CcP	apo CcP
$I(0)$ (from Guinier)	7.56	6.16
R_g (Å) (from Guinier)	20.36	20.27
$I(0)$ [from $p(r)$]	7.56	6.17
R_g (Å) [from $p(r)$]	20.32	20.17
D_{max} (Å)	56.77	52.29
Porod volume estimate (Å^3)	47 100	51 400
Molecular Mass Determination		
	holo CcP	apo CcP
SAXSMoW (kDa)	32.1	34.3
Q_R (kDa)	32.2	34.5
theoretical mass (kDa)	35.1	34.4
Model Statistics (q = 0.35 Å^{-1})		
	holo CcP	apo CcP
χ_{crysol}^2	1.12	1.19
χ_{free}^2	1.49	1.55
R_{SAS} (%)	0.0037	0.0188

essentially flat chemical shift perturbation profile (Figure 1C, right). This once again illustrates that Cc does not bind apo CcP.

Structural Comparison of Apo and Holo CcP. To understand the reason behind such a drastic difference in their binding properties, we sought to compare the three-dimensional structures of the two CcP forms. While multiple X-ray coordinates of holo CcP (and holo CcP−Cc complexes) are available in the PDB, to the best of our knowledge, structural characterization of apo CcP has not been reported. That is why we initially attempted to study this protein by X-ray crystallography and NMR spectroscopy. Unfortunately, in our hands, the dialysis method of Yonetani[5] has failed to produce diffraction-quality crystals of apo CcP, and extensive robotic screens of crystallization conditions have so far been unsuccessful. Moreover, low spectral quality, in particular poor signal dispersion, precluded structural analysis of apo CcP by solution NMR spectroscopy. Faced with these difficulties, we decided to pursue the study of this recalcitrant protein by small-angle X-ray scattering.

As shown in Figure 2A, the scattering curves of holo and apo CcP are very similar. In both cases, the SAXS data demonstrate that the scattering particles are globular, well-folded entities as indicated by the normalized Kratky plots (Figure 2A, inset).[32] Both CcP forms are monomeric in solution as their estimated molecular masses correspond to the respective theoretical masses. Indeed, the theoretical scattering curve calculated for the high-resolution crystal structure of the holo CcP monomer (PDB entry 1ZBY)[29] corresponds very well to the experimental SAXS data (Figure 2B,C and Table 1). Despite an overall similarity of the two scattering curves, the SAXS experiments

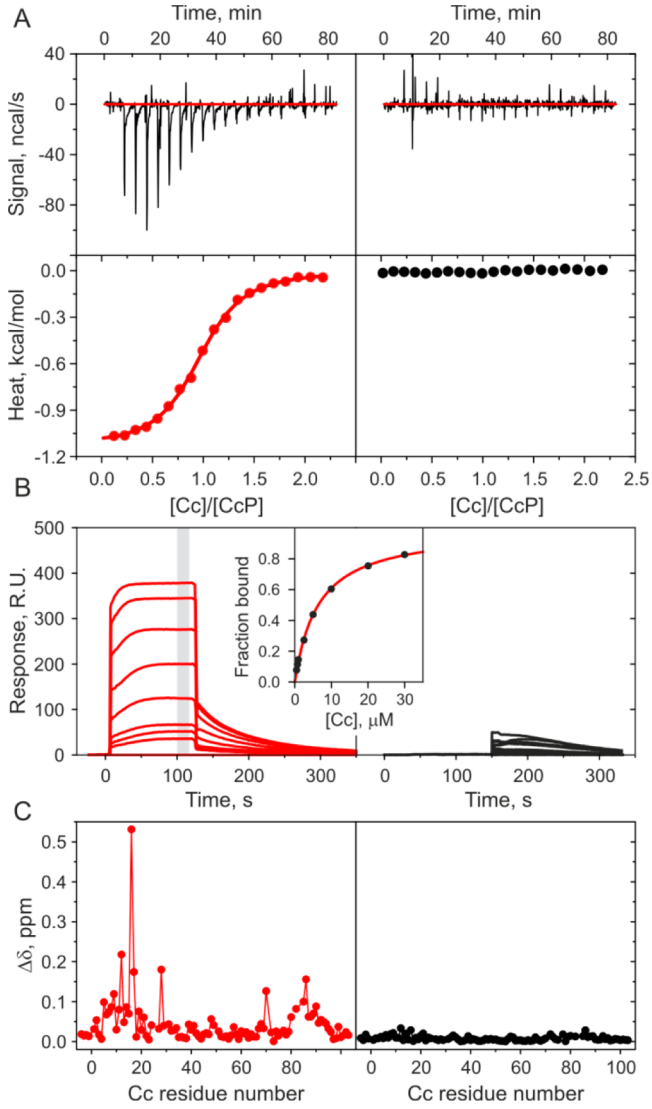

Figure 1. Cc binding properties of apo and holo CcP. Binding of holo CcP (left) and apo CcP (right) to ferric Cc observed by (A) isothermal titration calorimetry, (B) surface plasmon resonance, and (C) NMR spectroscopy. (A) The top and bottom panels show the raw data after baseline correction and the integrated data corrected for the heat of Cc dilution, respectively. The solid line in the bottom left panel represents the best fit of the holo CcP−Cc data to the 1:1 binding model with a K_D of 4.8 ± 0.2 μM. (B) Sensorgrams of the interaction of Cc with CcP immobilized on a CM5 chip collected at different Cc concentrations (see Materials and Methods). The gray area highlights the regions of the holo CcP−Cc sensorgrams used to determine the equilibrium response values (R_{eq}). The inset shows a plot of R_{eq} (expressed as the fraction of Cc bound) vs Cc concentration. The solid line represents the best fit to the 1:1 equilibrium binding model with a K_D of 6.4 ± 0.2 μM. (C) Average chemical shift perturbations ($\Delta\delta$) of Cc backbone amide resonances in the presence of 1 molar equiv of CcP. All experiments were conducted in 20 mM NaP_i and 100 mM NaCl (pH 6.0) at 25 °C.

indicate subtle differences in the solution behavior of apo and holo CcP. In particular, a closer inspection of the normalized Kratky plot reveals that the Porod invariant Q [corresponding to the area under the Kratky curve (Figure 2A, inset)] is smaller for apo than for holo CcP, suggesting that the former occupies a larger volume in solution. This finding is further confirmed by the Porod−Debye plot (Figure 2D), which may be used as a tool to distinguish flexibility from discrete conformational changes.[33]

dx.doi.org/10.1021/bi500603w | Biochemistry 2014, 53, 4526−4536

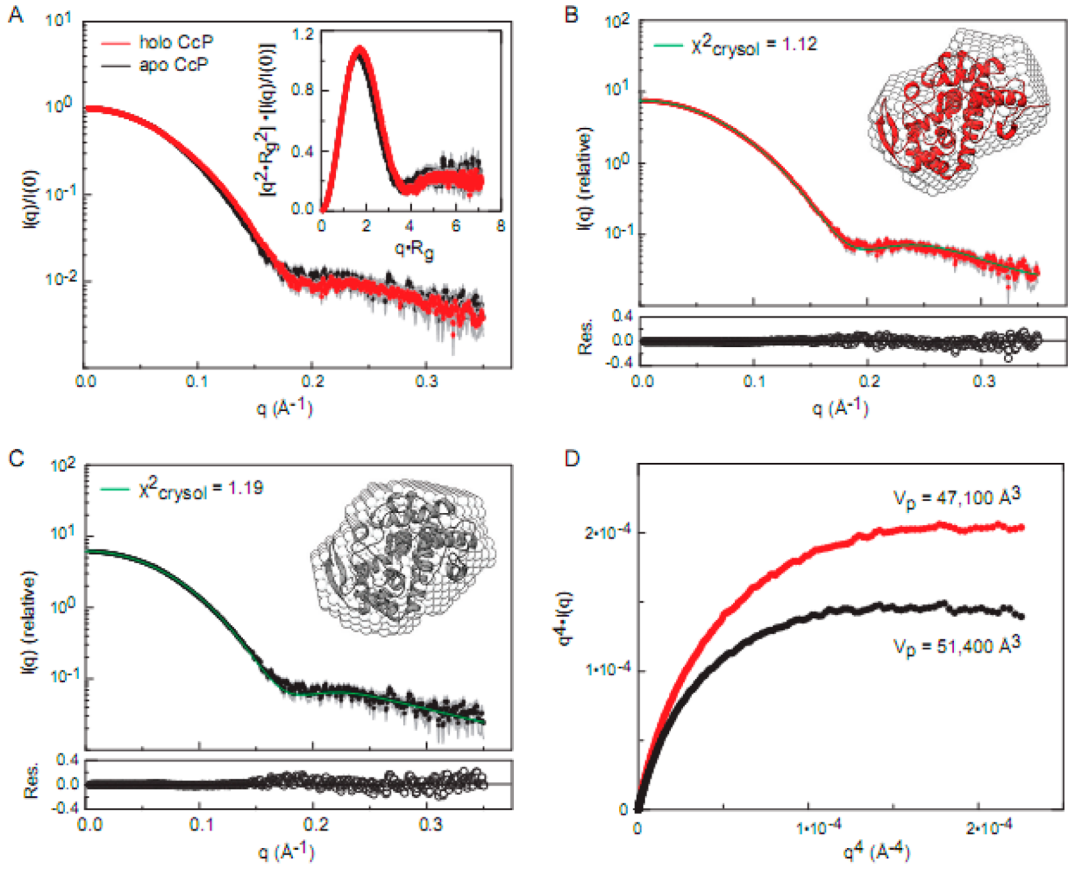

Figure 2. SAXS analysis of apo and holo CcP. (A) Zero-concentration scattering curves of apo and holo CcP (black and red, respectively). The error margins are colored gray. The inset shows the normalized Kratky plots. (B and C) Experimental scattering curves for (B) holo and (C) apo CcP. In both panels, the green line represents the CRYSOL fit for the CcP crystal structure (PDB entry 1ZBY);[29] the residuals of the fit to the experimental data are shown below. The inset shows an overlay of the CcP crystal structure (cartoon) and the *ab initio* model. (D) Porod–Debye plots for holo (red) and apo (black) CcP for the q range of 0.00549–0.12251 Å^{-1}. The estimated Porod volumes are indicated.

The Porod–Debye plot for apo CcP reaches a plateau at a lower value in comparison to that for holo CcP, indicating that apo CcP occupies a larger volume in solution. In conclusion, our SAXS experiments indicate that, although the global solution features displayed by apo and holo CcP are highly similar, holo CcP is more compact than apo CcP.

Thermal Denaturation. To further assess the differences between apo and holo CcP, we performed a series of equilibrium unfolding experiments. Thermal denaturation of apo and holo CcP was monitored by CD spectroscopy, with changes in the α-helical content followed at 222 nm. Both denaturation curves exhibit a single, cooperative unfolding event with similar melting temperatures (T_m) of 56.13 ± 0.02 °C for apo CcP and 58.03 ± 0.03 °C for holo CcP (Figure 3).

Urea-Induced Unfolding. Like the thermal denaturation presented above, a single, cooperative unfolding event is observed by CD spectroscopy for both apo and holo CcP with an increasing urea concentration (Figure 4). The transition midpoint (C_m) of 4.12 ± 1.72 M for apo CcP is somewhat higher than the C_m of 3.72 ± 0.92 M for the holo protein, yet the two values are the same within the error of the experiment.

Protein unfolding was also monitored by tryptophan fluorescence. For apo and holo CcP, addition of urea leads to a red shift in the fluorescence emission maximum, λ_{max}, indicating a progressive increase in the polarity of the medium surrounding the Trp residues, most likely due to the rising solvent exposure of the initially buried tryptophans that accompanies protein unfolding.[34] With λ_{max} values of 340.7 nm (apo) and 335.0 nm (holo) in the absence of urea, λ_{max} reaches 358.4 nm at 8 M urea for both proteins, corresponding to the red shifts ($\Delta\lambda_{max}$) of 18 and 23 nm for apo and holo CcP, respectively (Figure 5A). During the unfolding event, the fluorescence emission intensity,

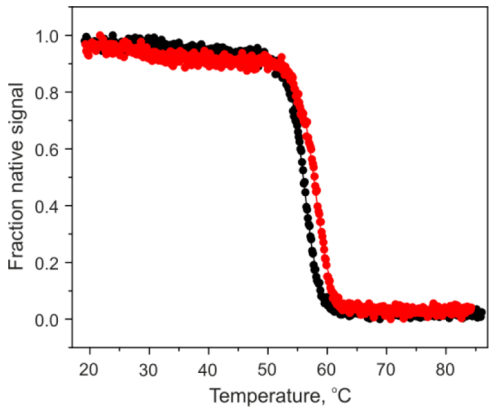

Figure 3. Thermal unfolding of apo and holo CcP monitored by CD spectroscopy. Black and red circles show changes in ellipticity at 222 nm of apo and holo CcP, respectively, in 20 mM NaP_i and 100 mM NaCl (pH 6.0) at increasing temperatures. Solid lines represent the best fits of the data to the two-state unfolding model (eq 2) with the following transition midpoints: T_m = 56.13 ± 0.02 °C (apo), and T_m = 58.03 ± 0.03 °C (holo).

dx.doi.org/10.1021/bi500603w | *Biochemistry* 2014, 53, 4526–4536

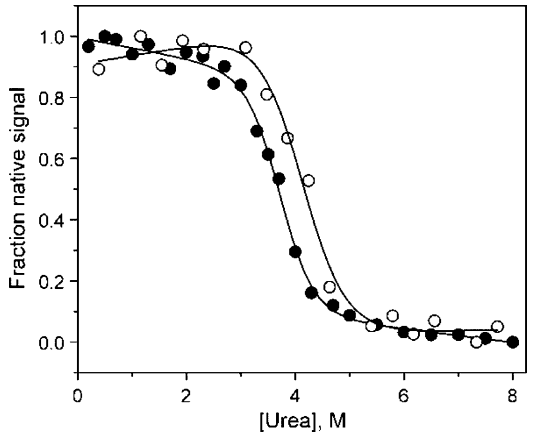

Figure 4. Urea unfolding of apo and holo CcP monitored by CD spectroscopy. Empty and filled circles show changes in ellipticity at 222 nm of apo and holo CcP, respectively, in 20 mM NaP_i and 100 mM NaCl (pH 6.0) at 25.0 ± 0.2 °C at increasing urea concentrations. Solid lines represent the best fits of the data to the two-state unfolding model (eq 3) with the following transition midpoints: C_m = 4.12 ± 1.72 M (apo), and C_m = 3.72 ± 0.92 M (holo).

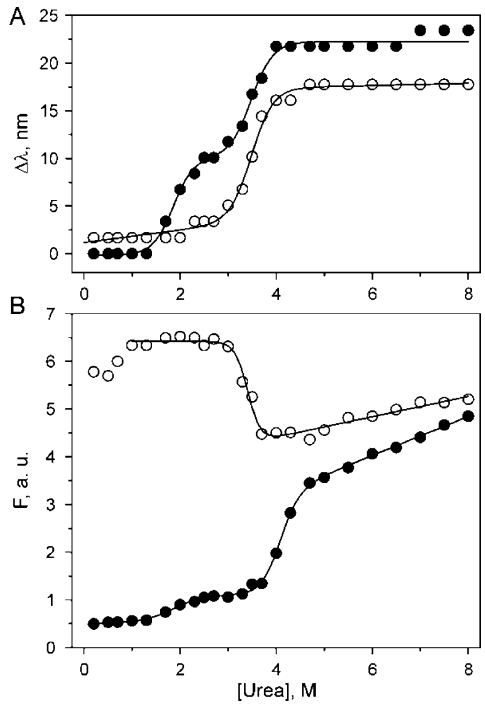

Figure 5. Urea unfolding of apo and holo CcP monitored by tryptophan fluorescence. Empty and filled circles show changes in the (A) position of the emission maximum and (B) the fluorescence intensity of apo and holo CcP, respectively, in 20 mM NaP_i and 100 mM NaCl (pH 6.0) at 25.0 ± 0.1 °C at increasing urea concentrations. Solid lines represent the best fits of the data to the model for two sequential, two-state unfolding steps (holo) or a single, two-state unfolding event (apo) (eq 3). The transition midpoints, given as the averages of the values derived from the data in the top and bottom plots, are 1.86 ± 0.31 M ($C_{m,1}$) and 3.77 ± 1.57 M ($C_{m,2}$) for the first and second events in the holo form, respectively, and 3.45 ± 1.13 M (C_m) for the apo form. Note that the first three points for apo CcP in panel B were excluded from the analysis.

F, of apo CcP decreases with an increasing urea concentration (Figure 5B, empty symbols), which is once again consistent with the rising polarity of the Trp environment.[34]

In contrast, unfolding of holo CcP is accompanied by an increase in *F* (Figure 5B, filled symbols). Of seven tryptophans present in CcP, two, W51 and W191, sit close to the heme group in the native holo protein, and thus, their fluorescence is expected to be effectively quenched by the cofactor. An increase in the Trp−heme separation and, eventually, dissociation of heme from the protein during the holo CcP unfolding event would lead to a decreased quenching of the fluorescence of W51 and W191, resulting in a higher *F*. At the same time, this trend is opposed by the decrease in *F* due to the increasing polarity of the Trp environment (as seen above for apo CcP). As a result, the actual fluorescence intensity is determined by the balance of these two counteracting effects. In the case of holo CcP, the decrease in the level of quenching by the heme appears to dominate the overall tryptophan fluorescence signal, leading to an increase in *F* with an increasing urea concentration (Figure 5B). Monitored by the changes in both λ_{max} and *F*, the denaturation curves for apo CcP exhibit a single unfolding event with an average C_m value of 3.45 ± 1.13 M, while those of holo CcP feature two transitions: an initial modest one followed by the much larger effect (Figure 5). The progress curves of holo CcP can be fit with the model describing two sequential, two-state unfolding events (eq 3), yielding the values $C_{m,1}$ = 1.86 ± 0.31 M and $C_{m,2}$ = 3.77 ± 1.57 M for the first and second transitions, respectively.

To characterize the two transitions observed for holo CcP by tryptophan fluorescence, we recorded UV−vis and NMR spectra of the protein at increasing urea concentrations. Monitored by the changes in the signal intensity at 380 and 415 nm, the denaturation curves clearly show two events, with transition midpoints of 1.65 ± 0.53 M ($C_{m,1}$) and 3.73 ± 0.78 M ($C_{m,2}$) (Figure 6A). As evidenced by the shift of the Soret band from 410 to 415 nm, the separation of the α and β absorption bands (536 nm and a shoulder at 568 nm), and the disappearance of the iron charge-transfer band at 647 nm, the first transition event involves conversion of high-spin $S = {}^5/_2$ holo CcP to a low-spin $S = {}^1/_2$ form (Figure 6B).[35,36] The NMR spectrum of holo CcP in 2.5 M urea reveals that the low-spin unfolding intermediate maintains considerable tertiary structure (Figure 7B). Accompanied by the shift of the absorption maximum to 396 nm and the disappearance of the α and β bands (Figure 6B), the second event comprises heme dissociation. Indeed, the UV−vis spectra at high urea concentrations look like combinations of those for a denatured protein and the free heme in an aqueous solution,[36] and the NMR spectrum features several clusters of strongly overlapping peaks at random-coil positions typical of a fully unfolded protein (Figure 7C).[37]

Gnd-HCl-Induced Unfolding. Monitored by the Trp fluorescence, unfolding of CcP by Gnd-HCl proceeds like that by urea: the red shift of λ_{max} is accompanied by progressive changes in the fluorescence emission intensity, which decreases for the apo form and increases for the holo protein (Figure 8A). However, unlike for the case of urea, the Gnd-HCl denaturation curves for both apo and holo CcP exhibit single transitions, with midpoints (C_m) of 1.34 ± 0.53 M (apo) and 1.40 ± 0.36 M (holo).

The changes in the UV−vis spectrum of holo CcP at increasing Gnd-HCl concentrations resemble those observed upon addition of urea. The progress curve exhibits two transitions, the first of which cannot be fit reliably, while the second, involving heme dissociation, is characterized by the midpoint value ($C_{m,2}$) of 1.43 ± 0.30 M (Figure 8B). It appears that the first, early onset transition event detected by UV−vis

dx.doi.org/10.1021/bi500603w | *Biochemistry* 2014, 53, 4526−4536

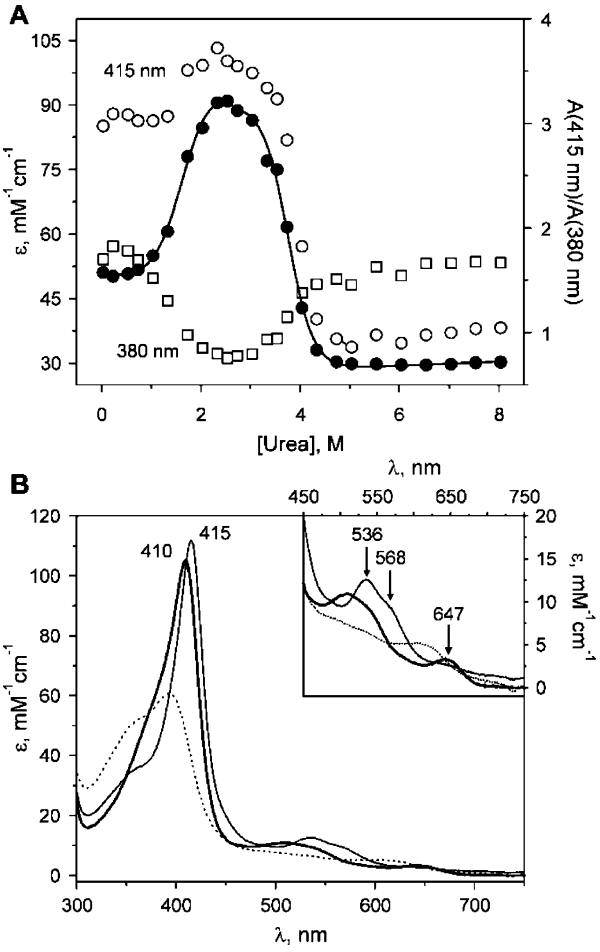

Figure 6. Urea unfolding of holo CcP monitored by UV−vis spectrophotometry. (A) The symbols show changes in absorption at 380 (□) and 415 nm (○) and the A_{415}/A_{380} ratio (●) of holo CcP in 20 mM NaP_i and 100 mM NaCl (pH 6.0) at 25.0 ± 0.2 °C at increasing urea concentrations. The solid line represents the best fit of the data to the model for two sequential, two-state unfolding steps (eq 3), with transition midpoints of 1.65 ± 0.53 M ($C_{m,1}$) and 3.73 ± 0.78 M ($C_{m,2}$) for the first and second events, respectively. (B) Electronic absorption spectra of holo CcP at different urea concentrations. The protein samples in 20 mM NaP_i and 100 mM NaCl (pH 6.0) at 25.0 ± 0.2 °C contained 0 M (thick solid line), 1.7 M (thin solid line), and 6.0 M urea (dotted line). The inset shows expansion of the 450−750 nm region. The positions of the absorption bands of high-spin $S = {}^5/_2$ holo CcP (0 M urea, thick solid line; Soret band at 410 nm and the iron charge-transfer band at 647 nm) and low-spin $S = {}^1/_2$ holo CcP (1.7 M urea, thin solid line; Soret band at 415 nm and α and β absorption bands at 536 and 568 nm) are indicated.

spectrometry is not resolved in the Trp fluorescence denaturation curve of the holo protein (Figure 8A).

Finally, protein unfolding was monitored by ANS fluorescence. Mimicking the native prosthetic group, ANS binds to apo CcP with a 1:1 stoichiometry, most likely occupying the vacant heme site as externally added heme was shown to replace CcP-bound ANS.[18] Increasing the concentration of apo CcP at a constant amount of ANS leads to a progressive increase in fluorescence intensity (Figure 8C, inset) and a gradual blue shift of the emission maximum (up to a $\Delta\lambda_{max}$ value of 33 nm), indicating that ANS interacts with a hydrophobic binding pocket.[38] Obtained from the ANS fluorescence titration (Figure 8C, inset), the K_D for the CcP−ANS interaction is 60 ± 6 μM, which is in good agreement with the K_D value of 55 μM for the apohemoglobin−ANS complex.[17] Addition of Gnd-HCl to the apo CcP−ANS complex leads to a gradual decrease in fluorescence intensity. The progress curve clearly shows an unfolding event at a C_m of 1.44 ± 0.24 M and perhaps an early onset transition similar to that observed by UV−vis spectrometry, which cannot be reliably fit (Figure 8C).

DISCUSSION

Protein Unfolding. Being typical for the cooperative unfolding of globular proteins, the sigmoid thermal denaturation profiles of apo and holo CcP feature single transition events (Figure 3). The T_m value of 58.03 °C for holo CcP is in excellent agreement with that obtained by differential scanning calorimetry (DSC) under closely matching experimental conditions (10 mM phosphate buffer, pH 6.0, and I = 100 mM).[39] Similar melting temperatures for apo and holo CcP suggest that the presence of the heme group has little effect on the overall protein stability, which is consistent with an early study by Asakura and Yonetani.[40] This conclusion is strengthened by the results of chemical unfolding monitored by CD spectroscopy and Trp fluorescence, showing that the transition midpoints, C_m, for urea or Gnd-HCl denaturation of apo and holo CcP are virtually the same. Overall, the C_m values obtained here by different techniques agree very well as can be seen for the unfolding of holo CcP by urea (C_m = 3.72−3.77 M from UV−vis, CD, and Trp fluorescence) and Gnd-HCl (C_m = 1.40−1.44 M from UV−vis, Trp fluorescence, and ANS fluorescence). The latter values are somewhat lower than the C_m of ∼2 M for the Gnd-HCl unfolding of holo CcP observed previously by CD spectroscopy,[41] most likely because of the differences in the experimental conditions.

Holo CcP Unfolding Intermediate. As can be clearly seen in the UV−vis urea denaturation profiles, unfolding of holo CcP is a two-step process (Figure 6A). Analysis of the spectral changes reveals that the two steps can be attributed to the high-spin to low-spin transition and the subsequent heme dissociation (see Results). The UV−vis spectra of holo CcP at increasing urea concentrations, as well as the overall denaturation curves, are very similar to those obtained in the thermal unfolding study of Gross and Erman,[36] who showed that the high-spin to low-spin conversion is reversible and hypothesized that it involves the ligation of heme by one of the distal residues, most likely H52.

The two holo CcP unfolding events are also observed by Trp fluorescence (Figure 5). Characterized by only a slight change in fluorescence intensity, the first transition is consistent with the increasing separation between the heme and one or both of the neighboring W51 and W191 groups, resulting in a modest reduction in the fluorescence quenching, which could accompany the changes in the heme spin state and coordination. This is followed by the second transition comprising cofactor dissociation and protein unfolding, which abolishes the Trp fluorescence quenching by the heme, giving rise to the pronounced effect. Overall, there is good agreement between the C_m values of the two transitions as seen by UV−vis and Trp fluorescence, indicating that the two techniques report on the same unfolding event.

As observed by UV−vis, the denaturation of holo CcP by Gnd-HCl also features two transitions, the first of which cannot be reliably fit (Figure 8B). This suggests that the same sequence of events takes place upon protein unfolding by Gnd-HCl as by urea, which, in turn, is in good agreement with the thermal denaturation profiles of Gross and Erman.[36] Furthermore, two

dx.doi.org/10.1021/bi500603w | Biochemistry 2014, 53, 4526−4536

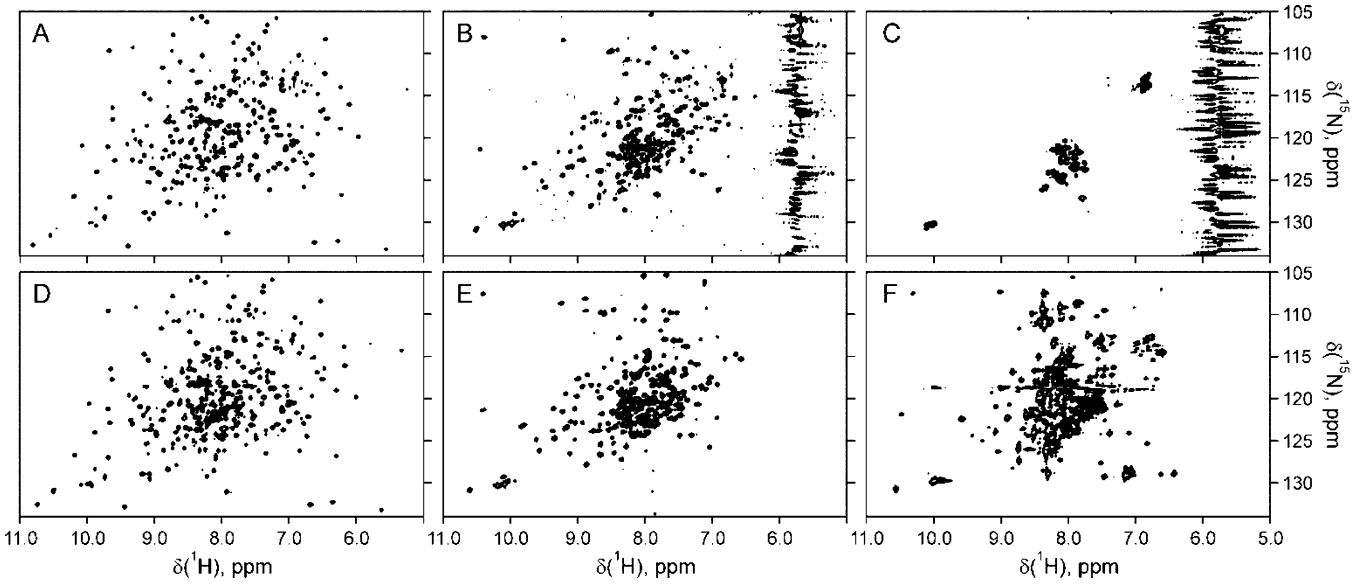

Figure 7. NMR spectra of apo and holo CcP under different denaturing conditions. (A–E) HSQC spectra of [^{2}H,^{15}N]holo CcP in 20 mM NaP_i and 100 mM NaCl at (A–C) pH 6.0 and 25 °C with (A) 0, (B) 2.5, and (C) 5 M urea; and (D and E) pH 7.0 and (D) 30 or (E) 45 °C. (F) HSQC spectrum of [^{2}H,^{15}N]apo CcP in 20 mM NaP_i and 100 mM NaCl (pH 6.0) at 25 °C.

unfolding transitions of holo CcP were described in the DSC study of Kresheck and Erman,[39] who showed that both endotherms displayed large enthalpy changes, the transition midpoint temperatures were similar to those observed by UV–vis spectrometry,[36] and the first transition was reversible while the second was not. To rationalize their findings, the authors proposed sequential unfolding of the two CcP domains. However, as evidenced by CD spectroscopy (Figures 3 and 4), the secondary structure of the holo protein does not change after the first transition event during urea unfolding ($C_{m,1}$ = 1.65–1.88 M as observed by UV–vis spectroscopy and Trp fluorescence in this work) or thermal denaturation ($t_{m1} \sim 50$ °C at pH 6.0 by DSC[39] or $t_{m1} \sim 38$ °C at pH 7.0 by UV–vis[36]). Instead, it seems more likely that the protein undergoes extensive reorganization of the native tertiary interactions, while the overall α-helical content is preserved. This alters the heme coordination and spin states, increases the separation between the heme and either one or both of the W51 and W191 residues, and explains the large enthalpy changes observed by DSC.[39]

Such reorganization of the native contacts in the unfolding intermediate is consistent with our NMR experiments, which show that holo CcP maintains considerable tertiary structure after the first unfolding transition. Featuring good signal dispersion typical for a globular protein, the NMR spectrum of holo CcP in 2.5 M urea is clearly different from those of the native protein and the fully denatured polypeptide (Figure 7A–C), indicating the formation of distinct tertiary contacts. To complement our study of the urea-induced CcP unfolding and characterize the first thermal transition event observed by UV–vis spectrometry[36] and DSC,[39] we recorded NMR spectra of holo CcP at 30 and 45 °C (pH 7.0), which correspond to the points before and after the transition, respectively (Figure 7D,E). As in the case of urea denaturation, the thermal unfolding intermediate appears to be distinct from native holo CcP and features the NMR spectrum typical of a protein with a well-defined tertiary structure. As evidenced by the overall similarity of the NMR spectra in panels B and E of Figure 7 (acquired at different pHs and temperatures), the thermal denaturation intermediate closely resembles that of urea unfolding. This observation reinforces our conclusion that unfolding of holo CcP by urea, Gnd-HCl, or temperature proceeds through the same sequence of events, following a very similar path from the native protein, via a distinct folded intermediate, to the fully denatured polypeptide.

In late 1960s, Yonetani and co-workers showed that binding of porphyrins to apo CcP occurs in two steps: the initial fast reaction (milliseconds to seconds) leads to the formation of a binding intermediate, which is then slowly converted to the final holo CcP (minutes).[5,40] The latter process was shown to be reversible and attributed to conformational changes in the apo protein required to accommodate the heme group. It is tempting to speculate that the heme binding intermediate of Yonetani and the holo CcP unfolding intermediate described here are the same species, suggesting the intriguing possibility that CcP navigates the same path on the energy landscape during inverse processes of cofactor-mediated protein folding and unfolding.

Structural and Hydrodynamic Properties of Apo CcP. Overall, the structural and hydrodynamic properties of apo CcP closely resemble those of the holo protein. As revealed by CD spectroscopy, both CcP forms possess the same secondary structure.[42] Furthermore, SAXS indicates that both apo and holo CcP behave as globular particles with nearly identical radii of gyration. At the same time, a thorough inspection of the SAXS data reveals that apo CcP occupies a larger molecular volume and, thus, is more expanded than the holo protein (Figure 2D and Table 1). This finding is consistent with earlier observations of a slight decrease in the sedimentation and diffusion coefficients and a small increase in the hydrodynamic radius of apo CcP compared to those of the holo form.[41,43] Furthermore, our results agree with conclusions of a more recent fluorescence spectroscopy study, which revealed that the vacant heme pocket in apo CcP is substantially solvent-exposed and suggested that the apo protein adopts an expanded, "opened-up" structure.[44] Finally, as exemplified by the binding of heme to apomyoglobin,[45] biliverdin to the lipocalin-type prostaglandin D synthase,[23] and abscisic acid to its binding protein PYR1,[33] the protein compaction upon cofactor binding observed in this work is not

dx.doi.org/10.1021/bi500603w | *Biochemistry* 2014, 53, 4526–4536

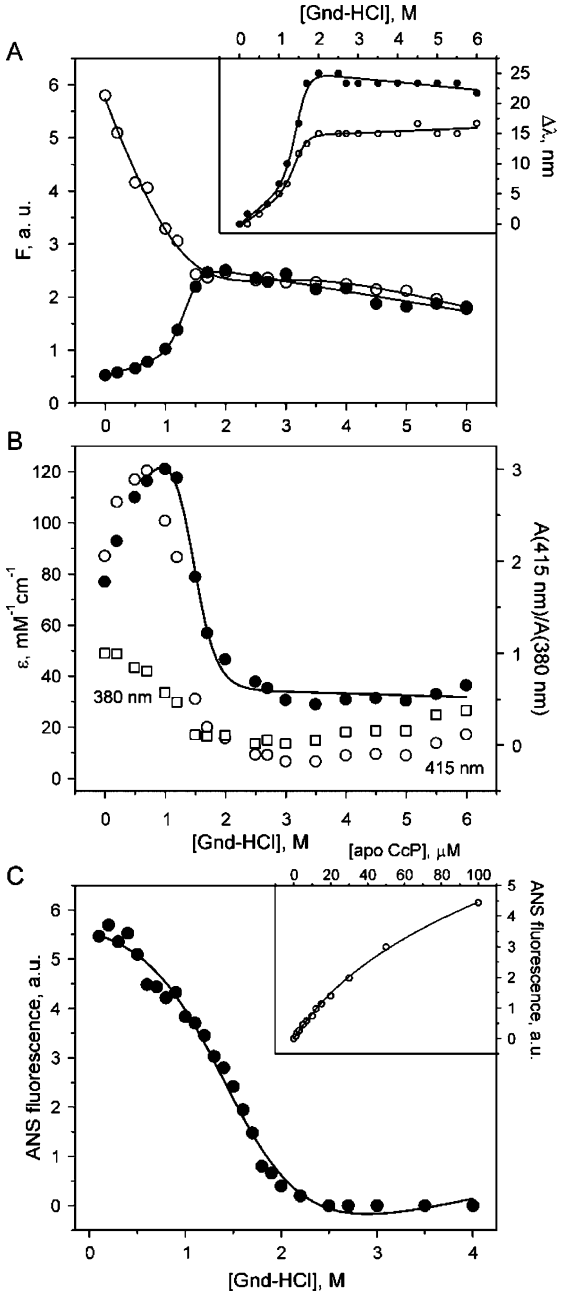

Figure 8. Gnd-HCl unfolding of apo and holo CcP. (A) Unfolding of apo and holo CcP monitored by tryptophan fluorescence. Empty and filled circles show changes in the fluorescence intensity (main plot) or the wavelength of the emission maximum (inset) of apo and holo CcP, respectively, in 20 mM NaP_i and 100 mM NaCl (pH 6.0) at 25.0 ± 0.1 °C at increasing Gnd-HCl concentrations. Solid lines represent the best fits of the data to the two-state unfolding model (eq 3). Averaged over the two data sets, the transition midpoints (C_m) are 1.34 ± 0.53 M (apo) and 1.40 ± 0.36 M (holo). (B) Unfolding of holo CcP monitored by UV−vis spectrophotometry. The symbols show changes in absorption at 380 (□) and 415 nm (○) and the A_{415}/A_{380} ratio (●) of holo CcP in 20 mM NaP_i and 100 mM NaCl (pH 6.0) at 25.0 ± 0.2 °C at increasing Gnd-HCl concentrations. The solid line represents the best fit of the data to the two-state unfolding model (eq 3), with a transition midpoint ($C_{m,2}$) of 1.43 ± 0.30 M. Note that the first unfolding transition could not be fit reliably; thus, the first four data points were omitted from the analysis. (C) Unfolding of apo CcP monitored by ANS fluorescence. Filled circles show changes in ANS fluorescence in the presence of apo CcP in 20 mM NaP_i and 100 mM NaCl (pH 6.0) at 25.0 ± 0.1 °C at increasing Gnd-HCl concentrations. The solid line represents the best fit of the data to the two-state unfolding model (eq 3), with a transition midpoint (C_m) of 1.44 ± 0.24 M. The inset shows the apo CcP-ANS titration fit to the binding model (eq 1), with the solid line indicating the best fit (K_D = 60 ± 6 μM).

specific to the CcP system and might represent a broader biophysical phenomenon.

Further differences between apo and holo CcP are revealed by NMR spectroscopy. While the HSQC spectrum of holo CcP features good signal dispersion and sharp resonances typical for a globular protein with a well-defined tertiary structure (Figure 7A), that of apo CcP shows poor resolution and broad peaks, indicating some structural disorder and/or extensive signal averaging due to conformational exchange (Figure 7F). Overall, apo CcP displays several characteristics attributed to the molten globule state:[46] a slightly expanded but still highly compact structure, native-like secondary structure content, greater surface accessibility to the solvent, and poor NMR signal dispersion and exchange broadening. However, unlike the true molten globule, apo CcP maintains a relatively well-ordered tertiary structure (as evidenced by SAXS and NMR), undergoes cooperative unfolding (with transition midpoints similar to those for the holo protein), and exhibits large enthalpy changes upon thermal denaturation.[39] Thus, apo CcP is better described as a "highly ordered molten globule" in Ptitsyn's terminology[47] or a "protein with partially-folded states" in the phrasing of Wright and co-workers.[48] It seems likely that a molten globule-like apo CcP resembles the unfolding intermediate of holo CcP (see above), which would explain why the single unfolding event of the apo protein (e.g., observed by DSC[39] or Trp fluorescence in this work) occurs at the transition midpoint matching that of the second event for holo CcP.

Studies of the apo forms of hemoproteins cytochrome b_5,[49] cytochrome b_{562},[46] heme oxygenase-1[50] and myoglobin[48] by X-ray crystallography and NMR spectroscopy demonstrate that all of them largely preserve the native secondary structure content and maintain a considerable tertiary structure, yet at the same time experience significant fluctuations and rearrangements of the heme binding pocket and exhibit varying degrees of dynamic disorder. In a similar vein, analysis of apo cytochrome $P450_{cam}$ by a combination of biophysical techniques showed that it adopted a partially destabilized native tertiary structure and displayed a folding intermediate-like character.[51] In general, it appears that all apo hemoproteins studied so far exhibit substantial structural plasticity and demonstrate properties associated with partially folded states. In this respect, apo CcP is a representative member of its class. Two conclusions, reached in the study of apomyogobin,[52] aptly summarize what we believe is also true for apo CcP: "... [apomyoglobin] has a molten-globule like character, its structure representing a population of interconverting substates rather than a fixed conformation", and "... addition of haem to apomyoglobin can be viewed as funneling a diverse, fluctuating population of substates into the native state". Among other things, such structural heterogeneity and inherent exchange dynamics could explain why numerous attempts to obtain diffraction-quality crystals of apo CcP by us and others have been unsuccessful (T. Poulos, personal communication).

Cc Binding Properties of Apo and Holo CcP. The observed differences between the fully folded, well-structured holo CcP and much more dynamic, molten globule-like apo protein could account for the striking disparity in the binding of

dx.doi.org/10.1021/bi500603w | Biochemistry 2014, 53, 4526−4536

the physiological partner, Cc. It seems likely that the Cc binding site present in the holo protein is disrupted in the apo form, which could explain why, while Cc interacts with holo CcP ($K_D \sim 5\ \mu M$ at $I = 115$ mM), its binding to apo CcP is completely abolished. Another system in which interactions of both apo and holo forms of a hemoprotein with its physiological partner were investigated is that of cytochrome b_5 (Cb_5) and cytochrome P450 (CYP).[53] In contrast to the Cc−CcP complex studied here, both apo and holo Cb_5 interact with CYP, engaging the same binding interface.[53] However, unlike apo CcP, apo Cb_5 appears to be much less disordered. In particular, its solution NMR structure showed only minor changes compared to that of the holo protein,[49] suggesting that Cb_5 largely preserves the native structure upon the removal of heme. These differences in the structural properties of apo Cb_5 and apo CcP could explain why the former maintains the binding to its interaction partner while the latter does not.

Interestingly, the contrasting binding properties of apo Cb_5 and apo CcP seem to be linked to their differing physiological functions and are likely biologically relevant. It is known that Cb_5 modulates the activity of many CYP isoforms, including the majority of the human drug-metabolizing CYPs.[54] One of the proposed activation mechanisms posits stimulation of the CYP activity by apo Cb_5, which was shown to hold true for some CYP isoforms.[54] Thus, the apo Cb_5−CYP interaction appears to be part of a normal physiological regulation network. At the same time, the enzymatically inactive apo CcP accumulates inside anaerobically grown yeast cells[7] and is able to undergo a rapid conversion to the fully active holo form upon aeration.[6,7] Triggered by the oxidative stress associated with the aerobic respiration, the post-translational activation of CcP most likely includes upregulation of genes governing heme biosynthesis and delivery, followed by insertion of the heme into apo CcP as part of an "induced conversion" mechanism.[6] This process yields mature holo CcP, which can interact with Cc to conduct the antioxidant enzymatic function. In this context, we suggest that the inability of apo CcP to bind Cc demonstrated in this work plays a distinct physiological role, allowing Cc to avoid an unproductive, wasteful interaction with inactive apo CcP in order not to limit its availability to other components of the mitochondrial redox chain.

AUTHOR INFORMATION

Corresponding Author

*E-mail: ovolkov@vub.ac.be. Telephone: (+32) 2 629 1025. Fax: (+32) 2 629 1963.

Funding

A.N.V. is an FWO Post-Doctoral Researcher. We acknowledge financial support from the VIB, and the Hercules Foundation for the purchase of the ITC machine.

Notes

The authors declare no competing financial interests.

ACKNOWLEDGMENTS

We thank Nico van Nuland for his help with the analysis of the unfolding curves, Abel Garcia-Pino for performing the ITC measurements, and Karen Van de Water for conducting preliminary unfolding experiments by CD spectroscopy.

ABBREVIATIONS

ANS, 8-anilinonaphthalene-1-sulfonic acid; Cb_5, cytochrome b_5; Cc, yeast iso-1-cytochrome *c*; CcP, yeast cytochrome *c* peroxidase; CD, circular dichroism; CpdI, Compound I; CYP, cytochrome P450; ET, electron transfer; HSQC, heteronuclear single-quantum coherence; ITC, isothermal titration calorimetry; SAXS, small-angle X-ray scattering.

REFERENCES

(1) Erman, J. E., and Vitello, L. B. (2002) Yeast cytochrome *c* peroxidase: Mechanistic studies via protein engineering. *Biochim. Biophys. Acta 1597*, 193−220.

(2) Volkov, A. N., Nicholls, P., and Worrall, J. A. R. (2011) The complex of cytochrome *c* and cytochrome *c* peroxidase: The end of the road? *Biochim. Biophys. Acta 1807*, 1482−1503.

(3) Altschul, A. M., Abrams, R., and Hogness, T. R. (1940) Cytochrome *c* peroxidase. *J. Biol. Chem. 136*, 777−794.

(4) Poulos, T. L., Freer, S. T., Alden, R. A., Edwards, S. L., Skogland, U., Takio, K., Eriksson, B., Xuong, N., Yonetani, T., and Kraut, J. (1980) The crystal structure of cytochrome *c* peroxidase. *J. Biol. Chem. 255*, 575−580.

(5) Yonetani, T. (1967) Studies on cytochrome *c* peroxidase: X. Crystalline apo- and reconstituted holoenzymes. *J. Biol. Chem. 242*, 5008−5013.

(6) Sels, A. A., and Cocriamont, C. (1968) Induced conversion of a protein precursor into cytochrome *c* peroxidase during adaptation of yeast to oxygen. *Biochem. Biophys. Res. Commun. 32*, 192−198.

(7) Djavadi-Ohaniance, L., Rudin, Y., and Schatz, G. (1978) Identification of enzymatically inactive apocytochrome *c* peroxidase in anaerobically grown *Saccharomyces cerevisiae*. *J. Biol. Chem. 253*, 4402−4407.

(8) Nicholls, P., and Mochan, E. (1971) Formation of a stable "active" complex between cytochrome *c* and yeast peroxidase. *Nat. New Biol. 230*, 276−277.

(9) Pelletier, H., and Kraut, J. (1992) Crystal structure of a complex between electron transfer partners, cytochrome *c* peroxidase and cytochrome *c*. *Science 258*, 1748−1755.

(10) Volkov, A. N., Worrall, J. A. R., Holtzmann, E., and Ubbink, M. (2006) Solution structure and dynamics of the complex between cytochrome *c* and cytochrome *c* peroxidase determined by paramagnetic NMR. *Proc. Natl. Acad. Sci. U.S.A. 103*, 18945−18950.

(11) Volkov, A. N., Vanwetswinkel, S., Van de Water, K., and van Nuland, N. A. J. (2012) Redox-dependent conformational changes in eukaryotic cytochromes revealed by paramagnetic NMR spectroscopy. *J. Biomol. NMR 52*, 245−256.

(12) Volkov, A. N., Wohlkonig, A., Soror, S. H., and van Nuland, N. A. J. (2013) Expression, purification, characterization, and solution nuclear magnetic resonance study of highly-deuterated yeast cytochrome *c* peroxidase with enhanced solubility. *Biochemistry 52*, 2165−2175.

(13) Yonetani, T., and Anni, H. (1987) Yeast cytochrome *c* peroxidase. Coordination and spin states of heme prosthetic group. *J. Biol. Chem. 262*, 9547−9554.

(14) Margoliash, E., and Frohwirt, N. (1959) Spectrum of horse-heart cytochrome *c*. *Biochem. J. 71*, 570−572.

(15) Delaglio, F., Grzesiek, S., Vuister, G. W., Zhu, G., Pfeifer, J., and Bax, A. (1995) NMRPipe: A multidimensional spectral processing system based on UNIX pipes. *J. Biomol. NMR 6*, 277−293.

(16) Vranken, W. F., Boucher, W., Stevens, T. J., Fogh, R. H., Pajon, A., Llinas, M., Ulrich, E. L., Markley, J. L., Ionides, J., and Laue, E. D. (2005) The CCPN data model for NMR spectroscopy: Development of a software pipeline. *Proteins 59*, 687−696.

(17) Stryer, L. (1965) The interaction of a naphthalene dye with apomyoglobin and apohemoglobin: A fluorescent probe of non-polar binding sites. *J. Mol. Biol. 13*, 482−495.

(18) Leonard, J. J., and Yonetani, T. (1974) Interaction of cytochrome *c* peroxidase with cytochrome *c*. *Biochemistry 13*, 1465−1468.

(19) van Nuland, N. A. J., Meijberg, W., Warner, J., Forge, V., Scheek, R. M., Robillard, G. T., and Dobson, C. M. (1998) Slow cooperative folding of a small globular protein HPr. *Biochemistry 37*, 622−637.

(20) Wiseman, T., Williston, S., Brandts, J. F., and Lin, L. N. (1989) Rapid measurement of binding constants and heats of binding using a new titration calorimeter. *Anal. Biochem. 179*, 131−137.
(21) Petoukhov, M. V., Franke, D., Shkumatov, A. V., Tria, G., Kikhney, A. G., Gajda, M., Gorba, C., Mertens, H. D. T., Konarev, P. V., and Svergun, D. I. (2012) New developments in the ATSAS program package for small-angle scattering data analysis. *J. Appl. Crystallogr. 45*, 342−350.
(22) Mangenot, S., Leforestier, A., Vachette, P., Durand, D., and Livolant, F. (2002) Salt-induced conformational and interaction changes of nucleosome core particles. *Biophys. J. 82*, 345−356.
(23) Miyamoto, Y., Nishimura, S., Inoue, K., Shimamoto, S., Yoshida, T., Fukuhara, A., Yamada, M., Urade, Y., Yagi, N., Ohkubo, T., and Inui, T. (2010) Structural analysis of lipocalin-type prostaglandin D synthase complexed with biliverdin by small-angle X-ray scattering and multidimensional NMR. *J. Struct. Biol. 169*, 209−218.
(24) Rambo, R. P., and Tainer, J. A. (2013) Accurate assessment of mass, models and resolution by small-angle scattering. *Nature 496*, 477−481.
(25) Fischer, H., de Oliveira Neto, M., Napolitano, H. B., Polikarpov, I., and Craievich, A. F. (2010) Determination of the molecular weight of proteins in solution from a single small-angle X-ray scattering measurement on a relative scale. *J. Appl. Crystallogr. 43*, 101−109.
(26) Franke, D., and Svergun, D. I. (2009) DAMMIF, a program for rapid *ab initio* shape determination in small-angle scattering. *J. Appl. Crystallogr. 42*, 342−346.
(27) Volkov, V. V., and Svergun, D. I. (1993) Uniqueness of *ab initio* shape determination in small-angle scattering. *J. Appl. Crystallogr. 36*, 860−864.
(28) Svergun, D. I. (1999) Restoring low resolution structure of biological macromolecules from solution scattering using simulated annealing. *Biophys. J. 76*, 2879−2886.
(29) Bonagura, C. A., Bhaskar, B., Shimizu, H., Li, H., Sundaramoorthy, M., McRee, D. E., Goodin, D. B., and Poulos, T. L. (2003) High-resolution crystal structures and spectroscopy of native and compound I cytochrome *c* peroxidase. *Biochemistry 42*, 5600−5608.
(30) Svergun, D. I., Barberato, C., and Koch, M. H. J. (1995) CRYSOL: A program to evaluate X-ray solution scattering of biological macromolecules from atomic coordinates. *J. Appl. Crystallogr. 28*, 768−773.
(31) Jacques, D. A., Mitchell Guss, J., Svergun, D. I., and Trewhella, J. (2012) Publication guidelines for structural modelling of small-angle scattering data from biomolecules in solution. *Acta Crystallogr. D68*, 620−626.
(32) Durand, D., Vivès, C., Cannella, D., Pérez, J., Pebay-Peyroula, E., Vachette, P., and Fieschi, F. (2010) NADPH oxidase activator p67phox behaves in solution as a multidomain protein with semi-flexible linkers. *J. Struct. Biol. 169*, 45−53.
(33) Rambo, R. P., and Tainer, J. A. (2011) Characterizing flexible and intrinsically unstructured biological macromolecules by SAS using the Porod-Debye law. *Biopolymers 95*, 559−571.
(34) Eftink, M. R. (1994) The use of fluorescence methods to monitor unfolding transitions in proteins. *Biophys. J. 66*, 482−501.
(35) Yonetani, T., Wilson, D. F., and Seamonds, B. (1966) Studies on cytochrome *c* peroxidase: VIII. The effect of temperature on light absorptions of the enzyme and its derivatives. *J. Biol. Chem. 241*, 5347−5352.
(36) Gross, M. T., and Erman, J. E. (1985) Thermal denaturation of cytochrome *c* peroxidase: pH dependence. *Biochim. Biophys. Acta 830*, 140−146.
(37) Dyson, H. J., and Wright, P. E. (2005) Elucidation of the protein folding landscape by NMR. *Methods Enzymol. 394*, 299−321.
(38) Rabbani, G., Ahmad, E., Zaidi, N., Fatima, S., and Khan, R. H. (2012) pH-induced molten globule state of *Rhizopus niveus* lipase is more resistant against thermal and chemical denaturation than its native state. *Cell Biochem. Biophys. 62*, 487−499.
(39) Kresheck, G. C., and Erman, J. E. (1988) Calorimetric studies of the thermal denaturation of cytochrome *c* peroxidase. *Biochemistry 27*, 2490−2496.
(40) Asakura, T., and Yonetani, T. (1969) Studies on cytochrome *c* peroxidase. XIII. Crystalline complexes of apoenzyme with porphyrins. *J. Biol. Chem. 244*, 537−544.
(41) Dowe, R. J., and Erman, J. E. (1985) Physicochemical characterization of the alkaline denaturation of cytochrome *c* peroxidase. *Biochim. Biophys. Acta 827*, 183−189.
(42) Sievers, G. (1978) Circular dichroism studies on cytochrome c peroxidase from baker's yeast (*Saccharomyces cerevisiae*). *Biochim. Biophys. Acta 536*, 212−225.
(43) Conroy, C. W., and Erman, J. E. (1978) pH titration study of cytochrome *c* peroxidase and apocytochrome *c* peroxidase. *Biochim. Biophys. Acta 537*, 396−405.
(44) Trammell, S. A., Jhaveri, S. D., LaBrenz, S. R., and Mauro, J. M. (2003) A comparative study of electrochemically and fluorometrically addressed molecular groups: Effects of protein microenvironment. *Biosens. Bioelectron. 19*, 373−382.
(45) Kataoka, M., Nishii, I., Fujisawa, T., Ueki, T., Tokunaga, F., and Goto, Y. (1995) Structural characterization of the molten globule and native states of apomyoglobin by solution X-ray scattering. *J. Mol. Biol. 249*, 215−228.
(46) Feng, Y., Sligar, S. G., and Wand, A. J. (1994) Solution structure of apocytochrome b_{562}. *Nat. Struct. Biol. 1*, 30−35.
(47) Ptitsyn, O. B. (1995) Structures of folding intermediates. *Curr. Opin. Struct. Biol. 5*, 74−78.
(48) Eliezer, D., and Wright, P. E. (1996) Is apomyoglobin a molten globule? Structural characterization by NMR. *J. Mol. Biol. 263*, 531−538.
(49) Falzone, C. J., Wang, Y., Vu, B. C., Scott, N. L., Bhattacharya, S., and Lecomte, J. T. J. (2001) Structural and dynamic perturbations induced by heme binding in cytochrome b_5. *Biochemistry 40*, 4879−4891.
(50) Sugishima, M., Sakamoto, H., Kakuta, Y., Omata, Y., Hayashi, S., Noguchi, M., and Fukuyama, K. (2002) Crystal structure of rat apoheme oxygenase-1 (HO-1): Mechanism of heme binding in HO-1 inferred from structural comparison of the apo and heme complex forms. *Biochemistry 41*, 7293−7300.
(51) Pfeil, W., Nölting, B. O., and Jung, C. (1993) Apocytochrome $P450_{cam}$ is a native protein with some intermediate-like properties. *Biochemistry 32*, 8856−8862.
(52) Lin, L., Pinker, R. J., Forde, K., Rose, G. D., and Kallenbach, N. R. (1994) Molten globule characteristics of the native state of apomyoglobin. *Nat. Struct. Biol. 1*, 447−452.
(53) Zhao, C., Gao, Q., Roberts, A. G., Shaffer, S. A., Doneanu, C. E., Xue, S., Goodlett, D. R., Nelson, S. D., and Atkins, W. M. (2012) Cross-linking mass spectrometry and mutagenesis confirm the functional importance of surface interactions between CYP3A4 and holo/apo cytochrome b_5. *Biochemistry 51*, 9488−9500.
(54) Schenkman, J. B., and Jansson, I. (2003) The many roles of cytochrome b_5. *Pharmacol. Ther. 97*, 139−152.
(55) Pernot, P., Thevenau, P., Giraud, T., Nogueira Fernandes, R., Nurizzo, D., Spruce, D., Surr, J., and McSweeney, S. (2010) New beamline dedicated to solution scattering from biological macromolecules at ESRF. *J. Phys.: Conf. Ser. 247*, 012009.